Large Eddy Simulations of the atmospheric boundary layer

Vincent Perrin

June 24, 2008

Abstract

In this study we have investigated the role of the subgrid model on the LES results of the stable boundary layer. The LES model was not suited to simulate the SBL, because the majority of the solutions were determined by the subgrid part of the model. The subgrid Prandtl number, given by $Pr = \frac{c_m}{c_h} = \frac{\phi_h}{\phi_m}$ was found to have a value of $\frac{1}{3}$, where field results measure a value around 1. By changing the subgrid Prandtl number from $\frac{1}{3}$ to 1 we have made the ratio ϕ_m to ϕ_h relations to become equal as obtained from field results. A second change made is the filter constant c_f, which determines the cutoff frequency of the subgrid filter. Changing this value from 2.5 to 2 increases the subgrid dissipation and decreases the resolved dissipation, and thereby making the subgrid part of the model becoming less dominant. Sensivity study to surface perturbation has revealed that the LES model solution is dependend on the geostrophic wind direction (i.e. large scale pressure gradient). Adding a small perturbation at the surface in the beginning of the simulation makes the thermals to reach the top of the domain where they lead to numerical instabilities. Adding the perturbation after a few hours can solve this problem. We can conclude that temperature heterogeneities at the surface increase the overall turbulence.

Contents

Chapter 1

Introduction

A large part of weather forecast model is dominated by the evolution of the atmosphere during the night. As we all know, the sun plays an important role in the dynamics of the atmosphere. Just before sunset, when the intensity of the incoming solar radiation decreases, the earth's surface starts to cool down as more radiation is emitted from the surface than is absorbed from the atmosphere. This process is know as radiative cooling and leads to a stable atmosphere with less vertical motion compared to the atmosphere during daytime. This atmospheric layer close to the ground is know as the stable (nocturnal) boundary layer and is still a problem to simulate. But the interest of simulating the stable boundary layer goes further then only the changes in the atmosphere during the night. Global climate models used to predict the climate on Earth are struggling with problems such as artic nights where the stable boundary layer remains for months. Improving the model for simulating the stable boundary layer would help improve the global climate models and make climate forecasts more accurate. This study will focus on the improvement of the Dutch Large-Eddy Simulation (DALES) and test the model sensitivity to surface temperature heterogeneities. Our objective is to match simulation data with field results.

Chapter 2

Analysis of the Large eddy Simulation model

In this chapter, the parts of the Large eddy Simulation (LES) model needed for this research will be discussed. For a full description of the LES, we can refer to the PhD thesis of Magreet van Zanten[11]. A LES model calculates the the evolution of the atmosphere in all three spatial dimensions. The main equation used is the Navier-Stokes equation, which gives a full description of the movement of liquid and gases. If we would be able to solve this equation analytically, we would be able to predict exactly the evolution of the atmosphere boundary layer (ABL). But unfortunately this equation remains unresolved even today. We can solve the Navier-Stokes equation numerically. In order to obtain this solution numerically, because of the nature of the Navier-Stokes equation, the Navier-Stokes equation needs to be solved on all scales, from the Kolmogorov micro scale ($\sim 1mm$) to the scale of the largest eddies present in the ABL ($\sim 1km$). Using a grid able to calculate the effect of all those scales would require a huge amount of computer power. The LES bypasses this problem by dividing the solution in two parts. The first part is the solution what has been explicitly calculated using the Navier-Stokes equation, restricted to the grid resolution. The second part is the subgrid part, which has been implemented to calculate the fluxes on a scale smaller then the grid. A good subgrid model should only have a small contribution to the total solution of the LES, and in ideal case should not influence him. The notation of van Zanten[11] will be used.

$$\tilde{x} = \langle x \rangle + x'' \tag{2.1}$$

with $< x >$ the resolved part and x'' the subgrid part. Although the governing equations are solved in each grid point, the output data of the LES model is horizontally (i.e. slab) averaged and will be denoted by using an overbar:

$$\langle x \rangle = \overline{\langle x \rangle} + \langle x \rangle' \tag{2.2}$$

Each part of the model will be discussed in more details in the next sections.

2.1 LES governing equations

As mentioned before, the resolved part of the solution is calculated using the Navier-Stokes equation:

$$\frac{\partial \langle u_i \rangle}{\partial t} + \frac{\partial \langle u_j \rangle \langle u_i \rangle}{\partial x_j} = - \frac{\partial \langle \pi \rangle}{\partial x_i} + g \frac{\langle \Theta_v \rangle}{\Theta_0} \delta_{i3} - \frac{\partial \tau_{ij}}{\partial x_j} - \delta_{i1} f (u_i - u_{gi}) + \delta_{i2} f (u_i - u_{gi}) \quad (2.3)$$

with δ_{ij} the Kronecker delta. θ_0 is the reference temperature and τ_{ij} the subgrid stress tensor is given by $\tau_{ij} = \langle \tilde{u}_j \tilde{u}_i \rangle - \langle u_j \rangle \langle u_i \rangle - 2/3\delta_{ij} \langle e \rangle$ with $\langle e \rangle$ the subgrid TKE. τ_{ij} is a consequence of filtering. The modified pressure π is defined as $\pi = \frac{\langle p \rangle}{\rho_0} + 2/3\langle e \rangle$. f is the Coriolis parameter and u_{gi} the geostrophic wind velocities in the u and v directions given by

$$fv_g = \rho^{-1} \frac{\partial \overline{p}}{\partial x} \quad (2.4)$$

$$fu_g = -\rho^{-1} \frac{\partial \overline{p}}{\partial y} \quad (2.5)$$

Another equation present in the resolved part is the filtered continuity equation:

$$\frac{\partial \langle u_i \rangle}{\partial x_i} = 0 \quad (2.6)$$

This equation assumes the incompressibility of air. A third equation present in the model is filtered conservation equation of thermal energy:

$$\frac{\partial \Theta_l}{\partial t} + \frac{\partial \langle u_i \rangle \langle \Theta_l \rangle}{\partial x_i} = \frac{\partial \langle u_i'' \Theta_l'' \rangle}{\partial x_i} - \frac{1}{\rho_0 c_p} \frac{\partial F}{\partial z} \quad (2.7)$$

where Θ_l is the liquid potential temperature and in absence of humidity is equal to the potential temperature. For more details we refer to van Zanten[11].

2.2 Subgrid scale parameterization

The subgrid fluxes of the conserved variables on a scale smaller than the grid resolution are parameterized. The use of the subgrid scale model is necessary to represent transport due to unresolved scales. But as it is only a approximation of the terms of the fluxes, only if the ratio of the SGS fluxes to the total fluxes is small, the LES can provide useful information. The subgrid fluxes are modeled as the product of a constant and a gradient. This closure is called the subgrid TKE closure and will be used in our model. Let us take a look at the main equation of this closure, where e is represents the subgrid TKE:

$$\frac{\partial \langle e \rangle}{\partial t} + \langle u_j \rangle \frac{\partial \langle e \rangle}{\partial x_j} = \frac{g}{\theta_o} \langle w'' \theta_v'' \rangle - \langle u_i'' u_j'' \rangle \frac{\partial \langle u_i \rangle}{\partial x_j} - \frac{\partial \langle u_j'' e \rangle}{\partial x_j} - \frac{1}{\rho_0} \frac{\partial \langle u_j'' p'' \rangle}{\partial x_j} - \epsilon \quad (2.8)$$

where p is the pressure and where the first part on the right hand side is the production/destruction of the buoyancy and the second is the production/destruction of the

wind shear. The third and fourth term are the transport terms. The fifth term is the subgrid viscous dissipation given by:

$$\epsilon = \frac{c_\epsilon \langle e \rangle^{3/2}}{\lambda} \tag{2.9}$$

with λ the typical length of the subgrid eddies and where c_ϵ is given by

$$c_\epsilon = \frac{2\pi}{c_f}\left(\frac{3}{2}\alpha\right)^{-3/2} \tag{2.10}$$

where c_f is a constant which determines the filter wavelength λ_f which is defined as $c_f\lambda$. c_f determines the cutoff wavelength of the subgrid filter. In order to solve the TKE subgrid equation (2.8), the subgrid fluxes are approximated as a product of an eddy viscosity K_m or eddy diffusivity K_h and the local gradient of the resolved variable. According to van Zanten[11] K_m and K_h, the subgrid parameters for the momentum and the heat transfer, are dependend on λ and on the square root of the subgrid TKE and can be written as follow:

$$K_m = c_m\lambda \langle e \rangle^{1/2} \qquad \text{with } c_m = \frac{c_f}{2\pi}\left(\frac{3}{2}\alpha\right)^{-3/2} \tag{2.11}$$

$$K_h = c_h\lambda \langle e \rangle^{1/2} \qquad \text{with } c_h = \frac{c_f}{2\pi}\left(\frac{3}{4}\beta\right)^{-1}\left(\frac{3}{2}\alpha\right)^{-1/2} \tag{2.12}$$

c_f is take equal to 2.5[11]. The ratio of the eddy viscosity and the eddy diffusivity is given by $\frac{K_m}{K_h} = \frac{c_m}{c_h} = \beta/2\alpha$, and is know as the turbulent Prandtl number. α and β follow from the turbulent spectrum of momentum and temperature.

Now let us analyse what the subgrid TKE equation (2.8) would lead to if the solution would be completely determined by the subgrid part[9]. In the LES the subgrid fluxes are modeled as follow

$$\langle u_i'' u_j'' \rangle = \tau_{ij} \equiv K_m\left(\frac{\partial \langle u_j \rangle}{\partial x_i} + \frac{\partial \langle u_i \rangle}{\partial x_j}\right) \tag{2.13}$$

$$\langle u_j'' \theta_l'' \rangle = -K_h\frac{\partial \langle \theta_l \rangle}{\partial x_j} \tag{2.14}$$

If we assume stable conditions in the SBL, the typical length scale λ of the turbulent eddies is given by:

$$\lambda = min\left(\Delta, c_n\frac{\langle e \rangle^{1/2}}{N}\right) \tag{2.15}$$

with c_n equal to 0.76 and Δ the representative grid size defined by

$$\Delta = (\Delta x \Delta y \Delta z)^{1/3} \tag{2.16}$$

Using the following substitutions, we will rewrite the TKE equation (2.8) after dividing the equation by $\langle 2e \rangle^{1/2}$ for computational efficiency reasons:

$$N^2 = \frac{g}{\theta_0}\frac{\partial}{\partial z}\left(A \langle \theta_l \rangle + B \langle q_t \rangle\right) \tag{2.17}$$

$$S^2 \equiv \left(\frac{\partial \langle u_j \rangle}{\partial x_i} + \frac{\partial \langle u_i \rangle}{\partial x_j}\right)^2 \tag{2.18}$$

where A and B are thermodynamical constants and q_t the total water.

The TKE equation (2.8) becomes:

$$\frac{\partial \langle e \rangle^{1/2}}{\partial t} + \langle u_j \rangle \frac{\partial \langle e \rangle^{1/2}}{\partial x_j} = \frac{1}{2 \langle e \rangle^{1/2}} \left[-K_h N^2 + \frac{1}{2} K_m S^2 - \frac{c_\epsilon \langle e \rangle^{3/2}}{\lambda} \right] \tag{2.19}$$

K_h and c_ϵ in equations (2.12) and (2.9) respectively are defined as follow:

$$c_h = \left(c_{h,1} + c_{h,2} \frac{\lambda}{\Delta} \right) c_m \tag{2.20}$$

and

$$c_\epsilon = c_{\epsilon,1} + c_{\epsilon,2} \frac{\lambda}{\Delta} \tag{2.21}$$

where the unknowns $c_{h,1}$, $c_{h,2}$, $c_{\epsilon,1}$, $c_{\epsilon,2}$ and c_m are model constants. When the atmosphere is moderately vertically stable,(i.e. $\lambda = \Delta$), the TKE equation (2.19) can be written as:

$$\frac{\partial \langle e \rangle^{1/2}}{\partial t} + \langle u_j \rangle \frac{\partial \langle e \rangle^{1/2}}{\partial x_j} = \frac{1}{4} c_m \Delta^2 S^2 \left[1 - (c_{h,1} + c_{h,2}) Ri_g \right] - \frac{(c_{\epsilon,1} + c_{\epsilon,2}) \langle e \rangle}{2\Delta} \tag{2.22}$$

where

$$Ri_g = \frac{N^2}{\frac{1}{2} S^2} \tag{2.23}$$

This leads to the steady-state solution of the subgrid TKE $\langle e \rangle$:

$$\langle e \rangle = \alpha S^2 \left(1 - (c_{h,1} + c_{h,2}) Ri_g \right) \tag{2.24}$$

where the proportionality factor α is given by: $\alpha = \frac{1}{2} \frac{c_m \left(\Delta x \Delta y \Delta z \right)^{2/3}}{c_\epsilon}$ This relation will later on be used to check if the solution is dominated by the subgrid part. Equation (2.24) is the same solution as founded with the Smagorinsky model, where the time derivative and the subgrid transport in equation (2.8) is taken as 0. From Baas et al.[1], we know that:

$$Pr = \frac{K_m}{K_h} = \frac{c_m}{c_h} = \frac{\phi_h}{\phi_m} = \frac{1}{c_{h,1} + c_{h,2}} \tag{2.25}$$

The ratio $\frac{\phi_h}{\phi_m}$ given by the TKE subgrid model is significantly different then the ratio calculated from field experiment results, where this ratio equals 1.

2.3 Background

First of all it is important to know what the atmospheric condition need to be in order to obtain a SBL. Just before sunset, the thermals in the convective boundary layer are shut off by a cooling surface. The potential temperature profile is characterized by a positive curvature and a temperature inversion at the top of the SBL (figure 4.1). This shallow stable layer of air is formed. This layer is characterised by a strong static stability and a low level of turbulence. Turbulence is mainly generated mechanically by vertical wind shear. A weak wind is present at the surface, but becomes supergeostrophic aloft. This wind profile is know as a nocturnal jet (figure 4.1) and is a consequence of the radiative cooling, which stratify the air, and decouples from the air above and becomes nearly frictionless and turbulence free and accelerates due to the pressure gradient. When equilibrium conditions are present, the Coriolis forced is balanced with the divergence of the vertical momentum flux, and accelerates the air even more resulting in a supergeostrophic wind. This wind tends to mix the stable layer under it. The vertical buoyancy flux present in the SBL has a linear shape (figure 4.1), according to the Nieuwstadt's 1-dimensional analysis.

First of all let us define what we have been calling the SBL. The depth of the SBL is defined using the surface momentum flux. The depth of the SBL is calculated by first determining the height at which the surface flux drops to 5% ($h_{0.05}$), followed by a lineair extrapolation (i.e. $h_{SBL} = \frac{h_{0.05}}{0.95}$). In order to analyse the results we will use the same parameters as used by Baas et al.[1] . According to this theory we can introduce a dimensionless stability parameter z/Λ,

$$\frac{z}{\Lambda} = \zeta = \frac{-\kappa z \frac{g}{\theta_v} \left\langle \overline{w'\theta_v'} \right\rangle}{u_\star^3} \tag{2.26}$$

where Λ is the local Obukhov length, $\left\langle \overline{w'\theta_v'} \right\rangle$ the flux of the potential temperature at a certain height and $u_\star$ is defined by $u_\star = \sqrt[4]{\overline{\langle u'w' \rangle}^2 + \overline{\langle v'w' \rangle}^2}$. Now we can define a dimensionless shear ϕ_m

$$\phi_m(\zeta) \equiv \frac{\kappa z}{u_\star} \sqrt{\left[\left(\frac{\partial \bar{u}}{\partial z}^2 \right) + \left(\frac{\partial \bar{v}}{\partial z} \right)^2 \right]} \tag{2.27}$$

and a dimensionless virtual potential temperature gradient ϕ_h

$$\phi_h(\zeta) \equiv \left(\frac{\kappa z}{\theta_\star} \right) \frac{\partial \overline{\theta_v}}{\partial z} \tag{2.28}$$

where $\theta_\star$ is defined as $\theta_\star = - \left\langle \overline{w'\theta_v'} \right\rangle / u_\star$. Due to the strong stratification present in the SBL, we can assume that the size of the eddies is not dependent on the height and thus z does not play a role in ζ for large values of $\frac{z}{\Lambda}$. According to Nieuwstadt[7] $\phi_{m,h}$ become linear functions and the following linear interpolations can be made[12] with $\phi_{m,h} = 1 + \beta_{m,h}\frac{z}{\Lambda}$, for a weakly stable atmosphere. We can use the Businger-Dyer function[4], which is $\phi_m = \phi_h = 1 + 5\frac{z}{\Lambda}$. Those relations derived from observations are strictly only valid for $\zeta < 1$, but can be a good approximation for larger values of ζ.

The stability of the SBL can be expressed as a function of a *gradient* Richardson number Ri_g defined as follow:

$$Ri_g = \frac{\left(\frac{g}{\overline{\theta_v}}\right)\frac{\partial \overline{\theta_v}}{\partial z}}{\left(\frac{\partial \overline{u}}{\partial z}\right)^2 + \left(\frac{\partial \overline{v}}{\partial z}\right)^2} \tag{2.29}$$

According to equation (2.29) this Richardson number is a scaled ratio between the buoyancy and the wind shear, and using ϕ_m (2.27) and ϕ_h (2.28) we can rewrite the gradient Richardson number as follow[3]:

$$Ri_g = \zeta \frac{\phi_h}{\phi_m^2} \tag{2.30}$$

Chapter 3

Case description

In this study we will compare our DALES model with other LES models. By this we hope to improve the LES model and try to match the data with experimental results. For the simulation boundary and initial conditions, the same as used by Beare et al[2] are used. The initial temperature profile consist of a mixed layer with potential temperature up to 100m with an overlying inversion of strength 0.01 Km^{-1}, and a surface cooling of 0.25 Kh^{-1} is used. The atmosphere is simulated during a period of 9h. The geostrophic wind is set to 8 ms^{-1} in the east-west direction to generate turbulence. A Coriolis parameter of $1.39 \cdot 10^{-4} s^{-1}$ is used, which corresponds to a latitude of 73°N. To increase turbulent motion a random potential temperature difference of 0.1 K and zero mean is applied to the first 50m of the domain. The vertical velocity at the bottom of the domain is maintained at zero, because a non-zero velocity would not be physically acceptable. In a stable atmosphere, gravity waves or buoyancy waves, can be generated when the adiabatic lapse rate is lower than the temperature gradient. Those waves are reflected at the top of the domain, a processes which does not occur in reality. To suppress this, gravity wave damping is applied above 300m, which is well above the turbulent layer, which has a height of approximatively 200m[2]. In order to compute the fluxes at the surface, Monin-Obukhov similarity is used, with constants $\beta_m = 5$ and $\beta_h = 8$, from equations (2.27) and (2.28), which is slightly different than the values used by Beare et al[2]. A domain size of 400m x 400m x 800m is used with a von Karman constant (κ) of 0.4.

A sensitivity study to surface heterogeneities will be performed by adding a surface temperature perturbation. Let us analyse why surface perturbations should have an impact on the dynamics of the SBL. From equation (2.3) it follows

$$\frac{\partial \langle w \rangle'}{\partial t} = \frac{g}{\theta_0} \langle \theta_v \rangle' \tag{3.1}$$

where the perturbation $\langle \theta_v \rangle'$ is given by

$$\langle \theta_v \rangle' = \langle \theta_v \rangle - \overline{\langle \theta_v \rangle} \tag{3.2}$$

From equation (3.1) we can see that vertical motion is generated by *horizontal* temperature perturbations. When we look at the boundary conditions of the LES we see that the surface temperature is homogeneous. This is certainly not true in the real world, where rivers can have different temperature.

Chapter 4

Modifications in the LES subgrid model

4.1 Problems with the reference model

In order to have an idea of how the SBL is behaving, let us take a look at some common[2] parameters, like temperature, wind speed and fluxes.
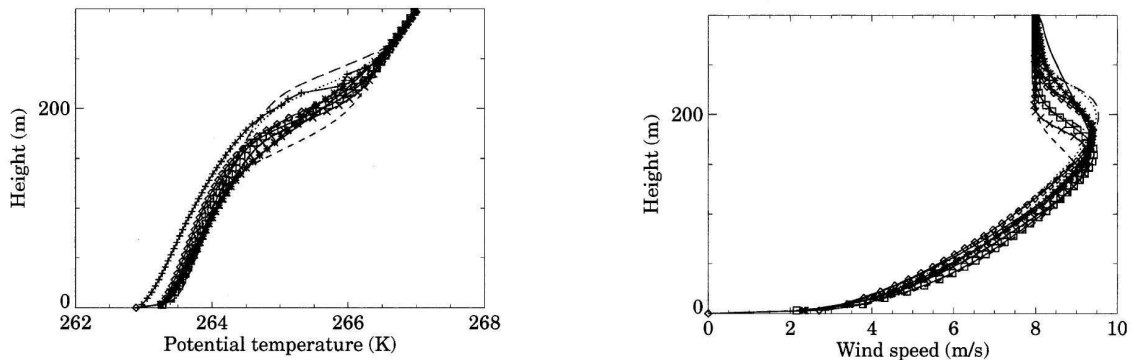

FIGURE 4.1: Typical potential temperature and wind profiles of a SBL from various LES models[2]

In figure 4.3 time series of the buoyancy flux, momentum flux, and SBL depth are shown. The SBL height stabilizes within 2 hours. The momentum flux takes more time to reach equilibrium and stabilizes after 4 hours. During the whole simulation is the surface cooling down, making it hard for the buoyancy flux to reach a steady state (figure 4.3). Even after 9 hours has the buoyancy flux not reach his equilibrium.

We will use the same model constants as van Zanten[11](4.1): Let us now compare our simulation results with those computed by Beare et al[2]. In this paper an intercomparison of different LES models is given. First of all we will look at some variables, averaged over the penultimate and ultimate hours of the simulation.

From figure 4.4 we can see that the temperature profile has the same shape, although the top of the temperature inversion is located at a height of 150m instead of 200m. The
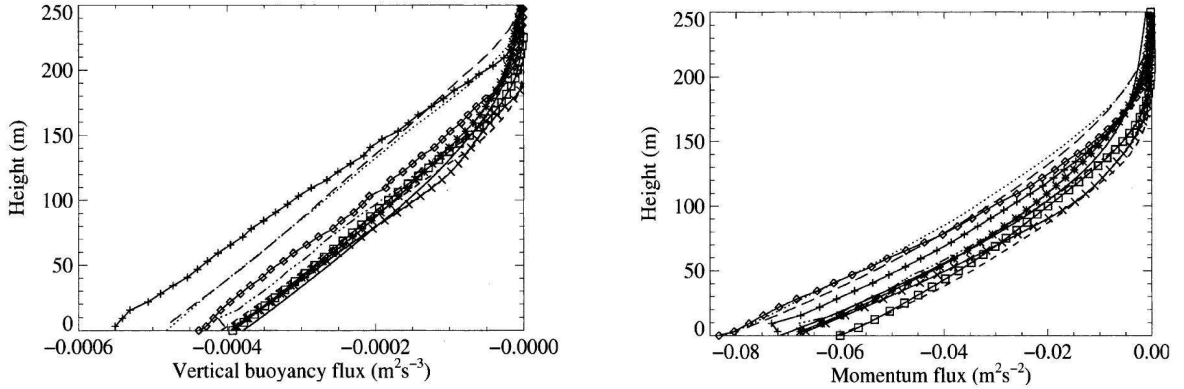
FIGURE 4.2: Typical vertical buoyancy and momentum profiles of a SBL from various LES models[2]

	ρ_0	α	β	c_ϵ	c_m	c_h	c_S	c_N	$\left(Ri_g\right)_c$
-	1.1436	1.5	1.0	0.70	0.12	$3c_m$	0.22	0.76	0.33
+				$c_{\epsilon,1} = 0.19$		$c_{h,1} = 1$			0.27
				$c_{\epsilon,2} = 0.51$		$c_{h,2} = 2$			

TABLE 4.1: Parameters used in our LES, with(+) and without (-) length scale correction.

temperature inversion can usually be found on top of the SBL. The mean wind profile looks roughly the same but the nocturnal jet peaks at a much lower height then expected (i.e. at 100m instead of 150m).

From figure 4.5 we can see that our vertical buoyancy profile has a larger value at the surface but when the height increases, decreases faster as found by Beare et al[2]. This means that the buoyancy fluxes are not transported well in our model and also that the subgrid model dominates. We can also see that the subgrid part dominates. In figure 4.6 a similar situation occurs in figure 4.5 when the height increases. The fluxes are too much damped in our model. We can also see that again the subgrid part dominates. By this we expect that the SBL depth will be smaller as can be seen in figure 4.7. Analysing the reference model has led to the conclusion that vertical transport is not as developed as it should be.

Let us now take a look at equation (2.24). This equation shows the analytical solution of the subgrid part of the LES model. As we can see from figure 4.9, the subgrid part of the TKE agrees with the theoretical solution of the model. We have found that the first level of data point does not agree with the theoretical solution and has been removed from the figure. It leads to the conclusion that the subgrid part of the model plays a dominating role. From the assumption that a subgrid model should not have a lot influence on the total solution, we can conclude that the used subgrid model is not suited for SBL simulation, when we are using a 6.25m grid size. If we lower the grid size, from equation (2.24), we know that we are also lowering the subgrid TKE. Another effect of a higher resolution is a more dominant resolved part. We are interested in the reason why other subgrid models can find reasonable results on a resolution of 6.25m, and why
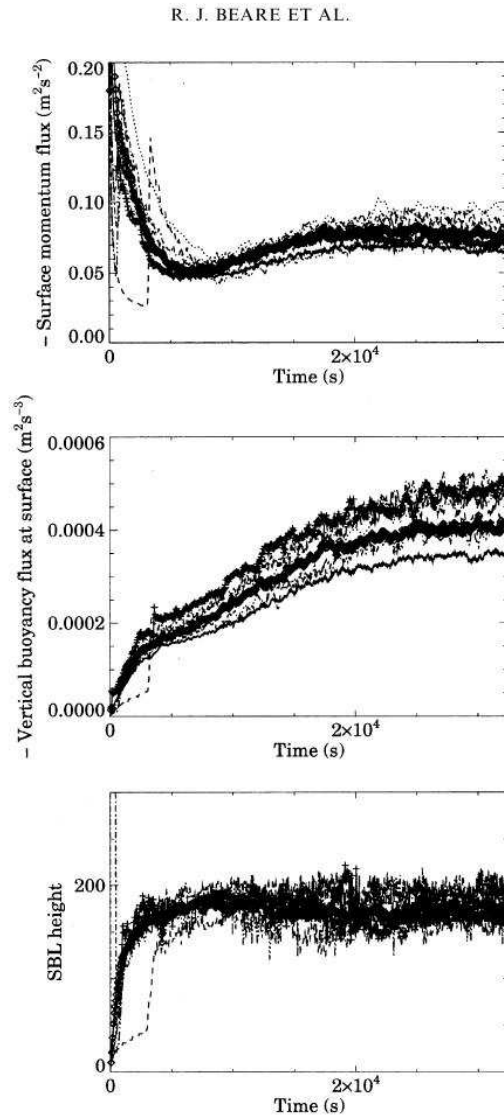
R. J. BEARE ET AL.

FIGURE 4.3: Typical time series for the momentum flux, buoyancy flux and the SBL depth from various LES models[2]
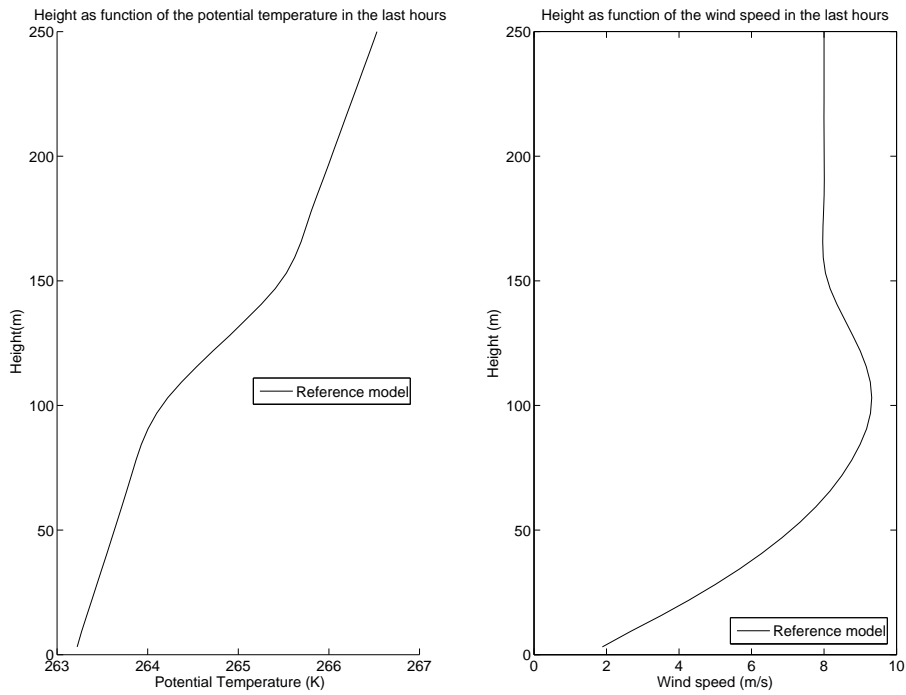
FIGURE 4.4: Mean potential temperature and wind profile profile of the reference model
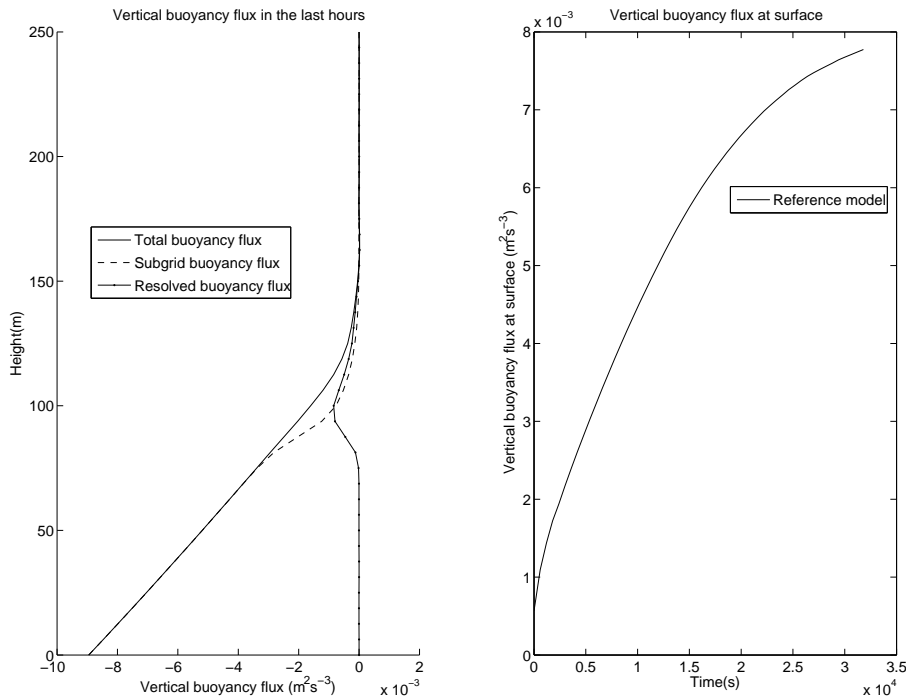
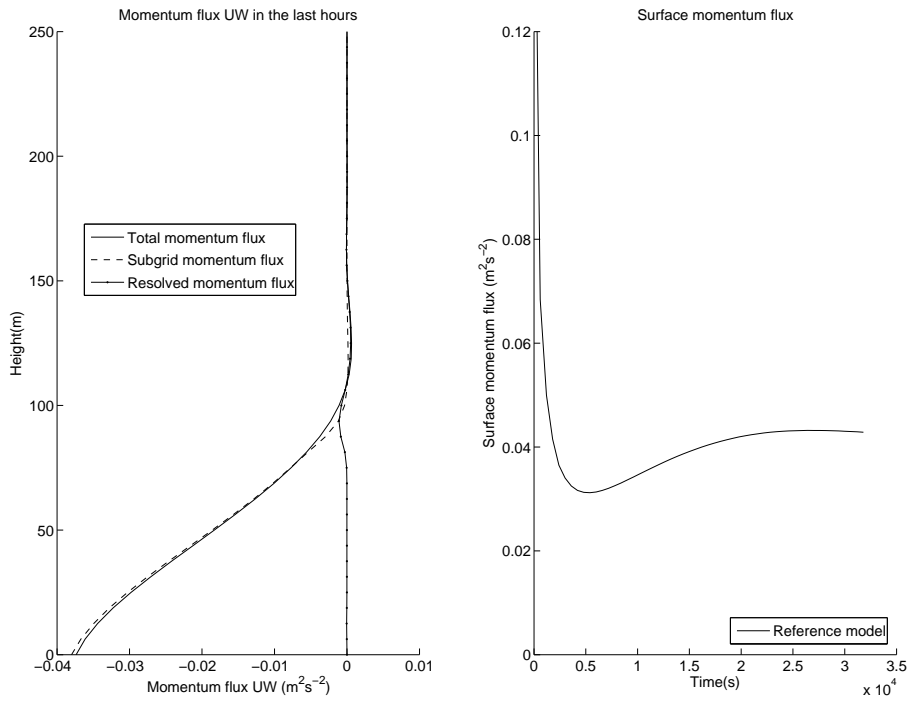FIGURE 4.5: Buoyancy flux at the surface and mean buoyancy profile of the reference model

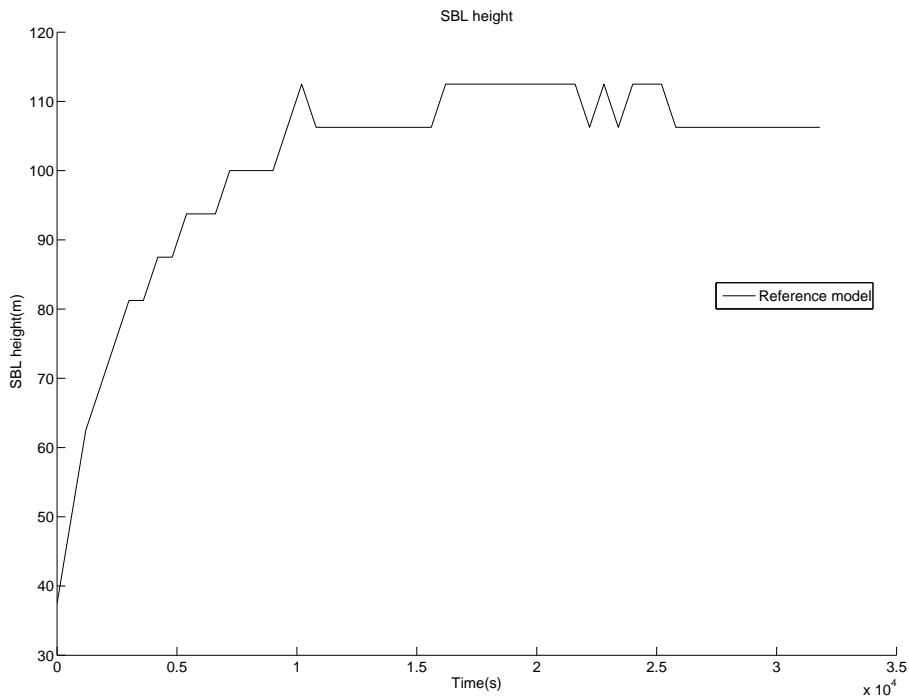FIGURE 4.6: Mean UW momentum flux profile and momentum flux at the surface of the reference model
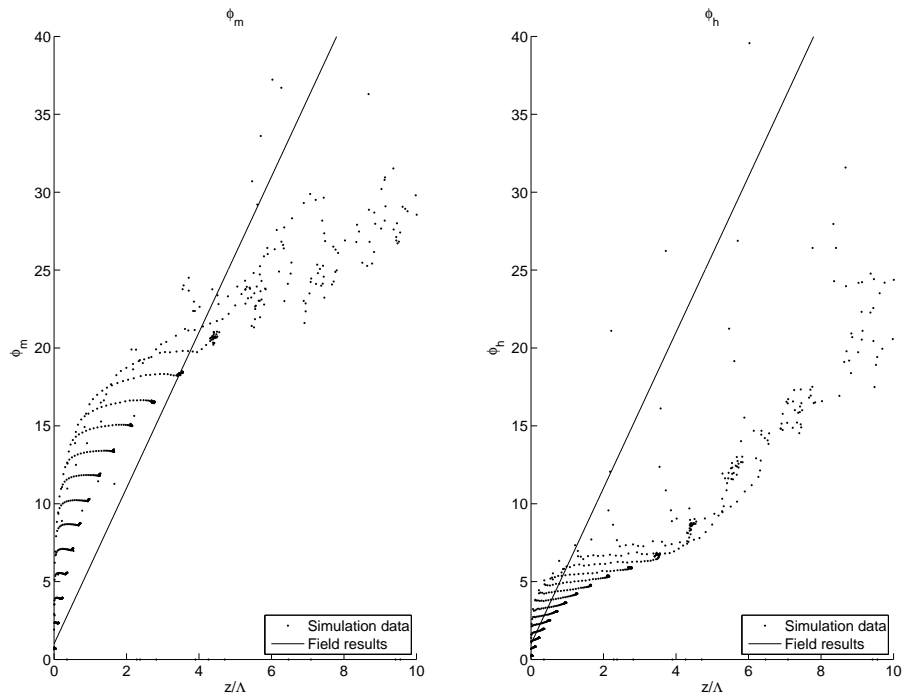

FIGURE 4.7: SBL depth of the reference model

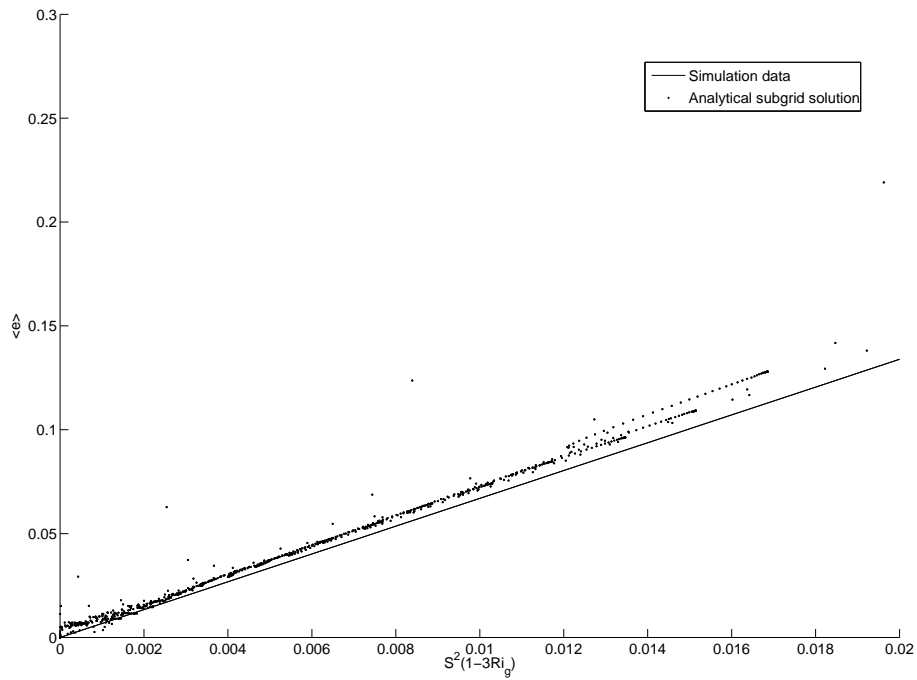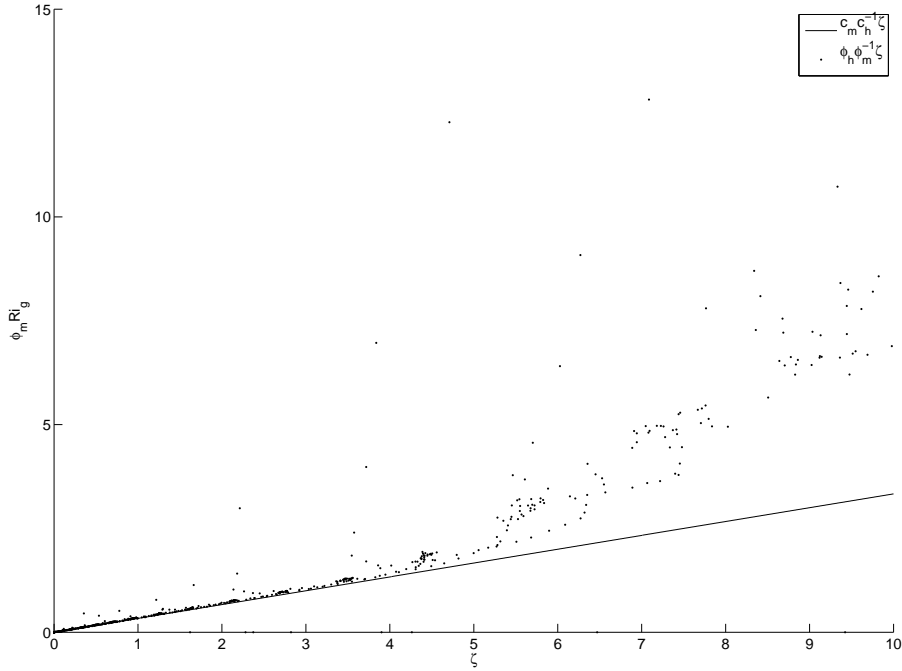FIGURE 4.8: ϕ_m and ϕ_h relations of the reference model

FIGURE 4.9: Plot of the subgrid TKE solution using the reference simulation

15

FIGURE 4.10: $\phi_m Ri_g$ as a function of ζ for the reference model

our results are almost fully subgrid determined. Now let us examine the ϕ_m and ϕ_h relation in order to understand what should be changed in the subgrid model to solve this problem. From figure 4.8, we can conclude that ϕ_m and ϕ_h are not in agreement with the observations. Only the data points present in the stable boundary layer have been plotted, because points above the SBL are not turbulent. Recalling equation (2.25), it is easily observed that the ratio of ϕ_m and ϕ_h is not equal to 1. Due to the non-linear shape of ϕ_m and ϕ_h lets us check if the results are consistent. A way to analyse the behaviour of both ϕ_m and ϕ_h is by rewriting equation (2.29) to $\phi_m Ri_g = \frac{1}{3}\zeta$ because we know that $\frac{c_m}{c_h}$ is implemented indirectly as $\frac{1}{3}$ in the subgrid model. This relation has been plotted in figure 4.10. For low values of ζ we see that $\phi_{h,m} = c_{m,h} = \frac{1}{3}$ as expected from the subgrid model analysis (section 2.2). This means that by investigating the ϕ_m and ϕ_h relations, the same conclusion can made as by observing figures 4.5, 4.6 and 4.9: The model we are using is dominated by the subgrid part.

Let us now search for a solution to improve the model. As mentioned before, field measurements give a Prandtl number approximately equal to 1 for stable conditions, but a value of $\frac{1}{3}$ is implemented in the subgrid model. From equation (2.25) we know also that that the Prandtl number is implemented in the LES as the ratio between c_m and c_h. Knowing this we can manually 'force' the model to have a Prandtl number of 1, to obtain results closer to reality. A length scale λ corrections is implemented to compute eddies with a size smaller than the representative grid size. This improves the subgrid solution by making it possible to compute eddies with a size less than the grid resolution. From the data of the reference model we can conclude that the turbulent eddies are not that small that a length scale correction λ is needed. This has been observed by looking at

16
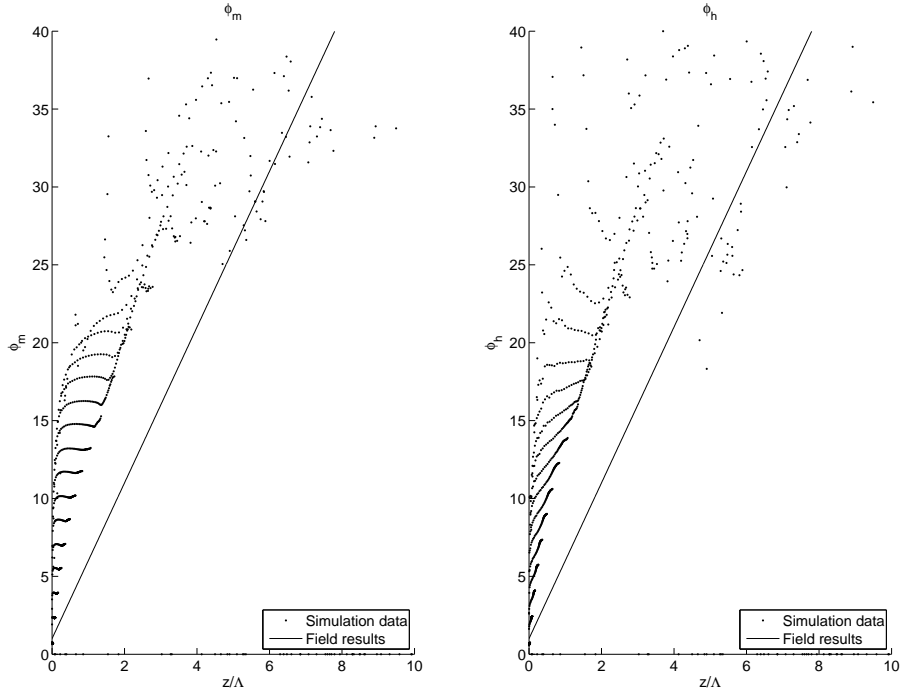
FIGURE 4.11: ϕ_m and ϕ_h relations with a subgrid Prandtl number of 1

the equation (2.15) and equation (2.20). If the size of the eddies would have been smaller than Δ, we would obtain a different relation for $\frac{K_m}{K_h}$, according to equation (2.20). This has not been observed, leading to the conclusion that, length scale correction was not needed. We can set the subgrid Prandtl number to 1 by changing the constants c_{h1} and c_{h2} to 1 and 0 respectively.

From figure 4.11 we can see that as implemented in the model, the ratio between ϕ_m and ϕ_h is around 1 for small values of $\frac{z}{\Lambda}$. But this implementation has not improved the results, as the data still do not coincide with the field results. The value of $\phi_{m,h}$ is larger than the value observed. This implies that λ is always equal to Δ and thus equation (2.21) will always be $c_\epsilon = c_{\epsilon 1} + c_{\epsilon 2}$ in our simulation. Knowing this we can put $c_{\epsilon 2}$ to 0 and $c_{\epsilon 1}$ to 0.7 for this simulation.

4.2 Improved reference model

In our model we used the same c_f as used by van Zanten[11] (i.e. 2.5). But as mentioned in her PhD thesis, other LES model use $c_f = 2$ (e.g. Mason[6]). Changing this constant can be a solution to improve the subgrid model. Let us take a look at the consequences of changing c_f. In tabel 4.2 we have not included the length scale correction λ because the SBL is not stable enough to enter the required regime. The constants have been calculated using equations (2.11) and (2.12). Using the constants as mentioned in table 4.2, we obtain the results for the relations ϕ_m and ϕ_h as can be seen in figure 4.12. Using the constants from tabel 4.2 has greatly improved the results from the LES model. In

ρ_0	α	β	c_ϵ	c_m	c_h	c_S	c_N
1.1436	1.5	1.0	$c_\epsilon = 0.875$	0.096	c_m	0.22	0.76
			$c_{\epsilon,1} = 0.875$		$c_{h,1} = 1$		
			$c_{\epsilon,2} = 0$		$c_{h,2} = 0$		

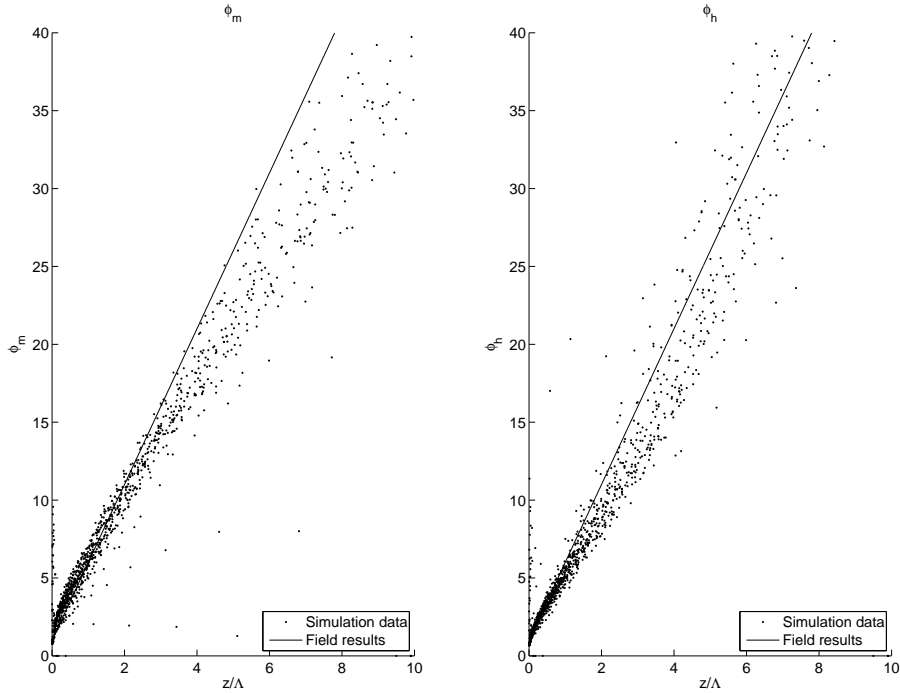TABLE 4.2: Parameters used to improve the subgrid model

FIGURE 4.12: ϕ_m and ϕ_h relations of our new reference model

figure 4.12 the LES data matches nicely with observation results. Although the ϕ_m and the ϕ_h relations looks nice, let us check them as we did before with equation (2.29) We can see from figure 4.13, the data is consistent for $\zeta < 5$. For higher values of ζ the data start to diverge. As we did before, let us compare the common parameters to analyse the changes. From the mean temperature profile from figure 4.14 we can see that changing c_f and forcing the Prandtl number to be 1 has shifted the inversion height. From this change we can conclude that vertical mixing in the SBL is improved as wanted. A higher nocturnal jet means that momentum transport is improved. Let us now take a look at the fluxes.

From figure 4.16, we can conclude that changing the value of the Prantl number has a negligible effect on the vertical momentum fluxes (i.e. the mean profile and at the surface). But in addition changing c_f facilitates the vertical transport of momentum, increasing the amplitude and the height of the transport. Changing the Prandtl number has led to a less negative buoyancy flux (figure 4.15). But in the improved reference model the vertical buoyancy fluxes (i.e. the mean profile and at the surface) are greater and reach
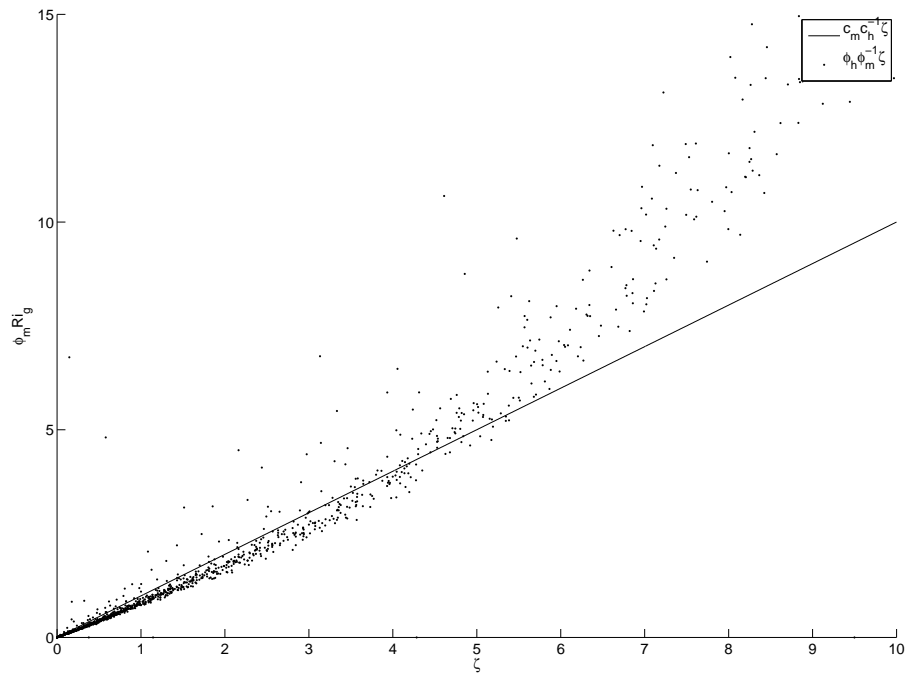
FIGURE 4.13: $\phi_m Ri_g$ as a function of ζ for the improved reference model
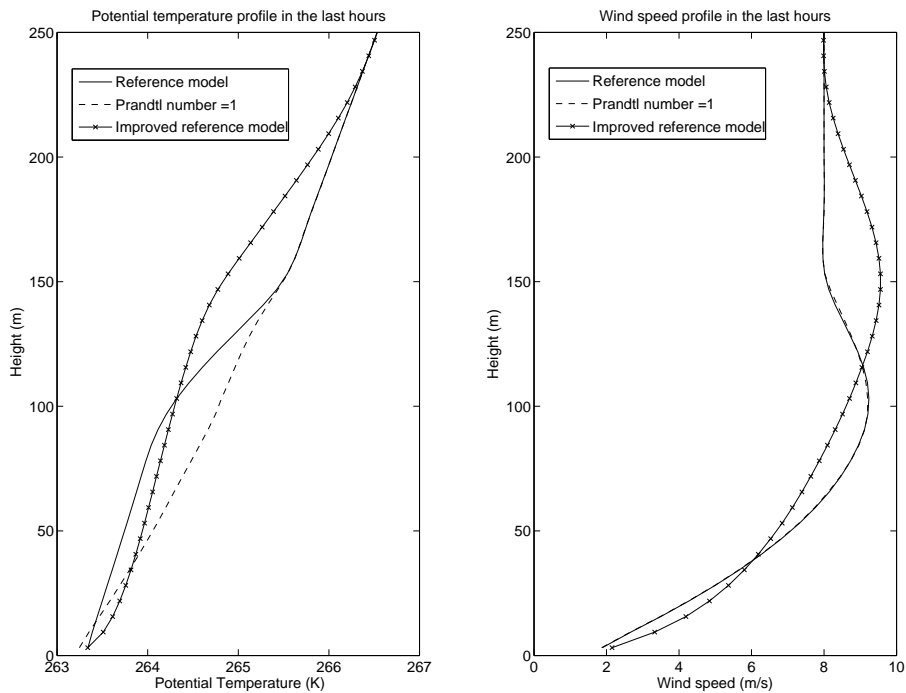

FIGURE 4.14: Mean potential profile and wind profile of the three different model settings
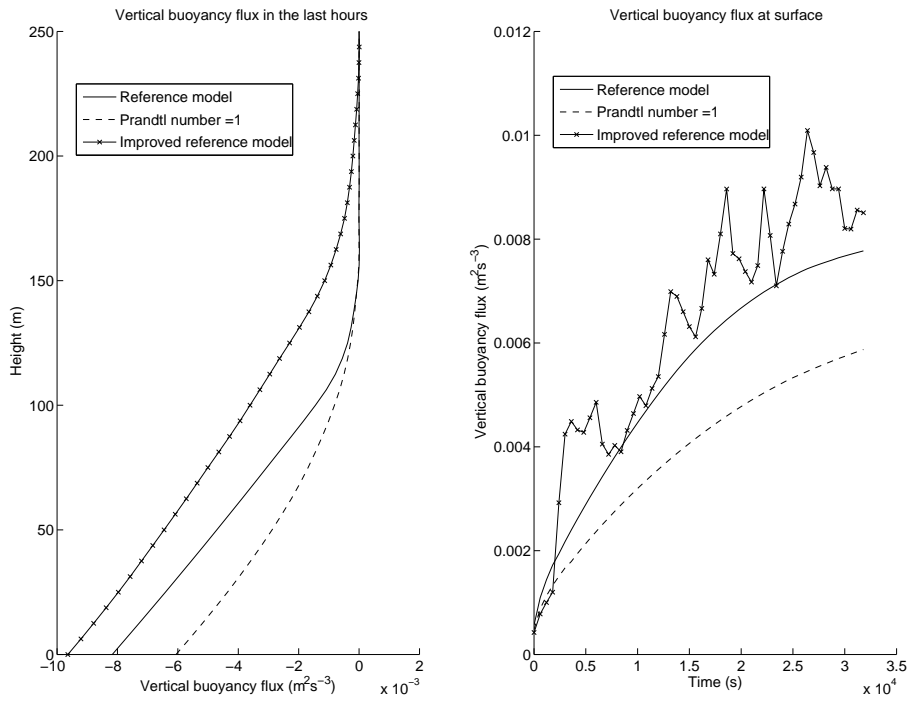
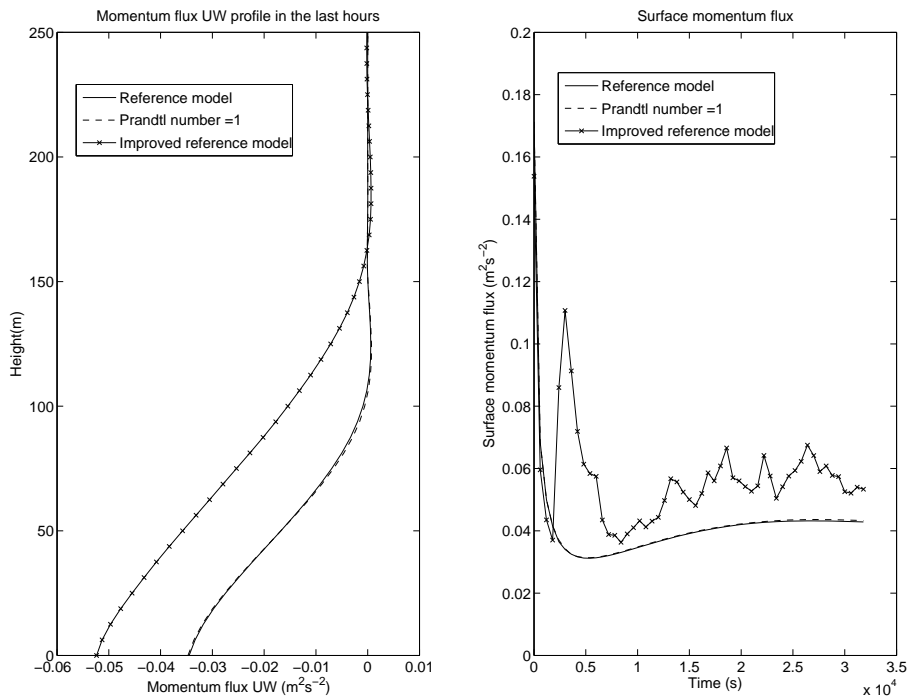FIGURE 4.15: Surface momentum flux of the three different model settings

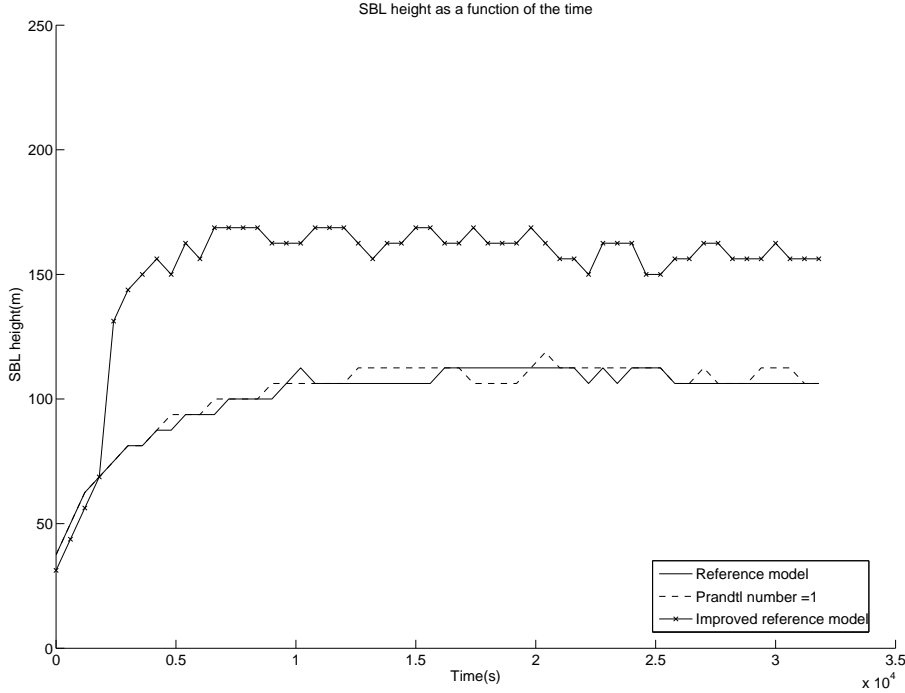FIGURE 4.16: Surface momentum flux of the three different model settings

FIGURE 4.17: SBL depth of the three different model settings

a greater height before vanishing. As we can see from figure 4.12, the change of the constant c_f (i.e. from 2.5 to 2) has been beneficial for the momentum and the buoyancy flux. In addition, both ϕ_m and ϕ_h relations agree with the experimental field results. We can see that changing c_f to a value of 2, has decreased the slope of both $\phi_{m,h}$ relations. The SBL depth increases significantly due to the change of c_f and is now in agreement with figure 4.3.

We can now ask ourself why the change of c_f has improved the simulation data. First let us take a look at equation (2.8), (2.9) and (2.21) giving the subgrid dissipation. Lowering c_f has a direct influence on both. From the equations for the eddy diffusivity of the heat and the eddy viscosity of the momentum (2.11) and (2.12) we know that lowering c_f lowers the value of $c_{m,h}$ and thereby lowers the value of $K_{m,h}$. This leads to less subgrid turbulent transport. The subgrid TKE balance is given by equation (2.8) where the dissipation is given by equation (2.9) and (2.21). Lowering the value for c_f increases the subgrid dissipation, and thus *suppresses* the subgrid solution. But only suppressing the subgrid part does not improve the model, especially if all the motion is calculated by the subgrid model. Changing c_f also has a impact on the resolved solution because the subgrid dissipation is directly connected to the resolved solution. This can be seen from observing equation (3.1). The *dissipation* of resolved TKE is roughly equal to the *production* of subgrid TKE. Here follows a part of the derivation from de Roode[8] beginning with the prognostic equation (2.3) for the resolved velocity. Using Reynolds decomposition this equation can be rewritten as:

21

$$\frac{\partial \overline{\langle u_i \rangle'^2}}{\partial t} + \overline{\langle u_j \rangle} \frac{\partial \overline{\langle u_i \rangle'^2}}{\partial x_j} = 2\frac{g\delta_{i3}}{\theta_0} \overline{\langle u_i \rangle' \langle \theta_0 \rangle} - 2\overline{\langle u_i \rangle' \langle u_j \rangle'} \frac{\partial \overline{\langle u_i \rangle}}{\partial x_j} - 2\overline{\langle u_i' \rangle \frac{\partial \langle \pi' \rangle}{\partial x_i}} -$$

$$\frac{\partial \overline{\langle u_i \rangle' \langle u_i \rangle' \langle u_j \rangle'}}{\partial x_j} + 2\overline{\langle u_i \rangle' \frac{\partial}{\partial x_i} \left((\langle K_m \rangle + K_m') \left(\frac{\partial \langle u_i \rangle'}{\partial x_j} + \frac{\partial \langle u_j \rangle'}{\partial x_i} \right) \right)} \qquad (4.1)$$

The last part of equation 4.1 is the resolved dissipation computed in the LES model and can be decomposed in 3 terms

$$\overline{2\langle u_i \rangle' \frac{\partial}{\partial x_i} \left((\langle K_m \rangle + K_M') \left(\frac{\partial \langle u_i \rangle'}{\partial x_j} + \frac{\partial \langle u_j \rangle'}{\partial x_i} \right) \right)} = \overline{-2(\langle K_m \rangle + K_m') \left(\frac{\partial \langle u_i \rangle'}{\partial x_i} \right)^2} +$$

$$2\frac{\partial}{\partial x_j} \left(\langle u_i \rangle' (\langle K_m \rangle + K_m') \left(\frac{\partial \langle u_i \rangle'}{\partial x_j} + \frac{\partial \langle u_j \rangle'}{\partial x_i} \right) \right) - 2(\langle K_m \rangle + K_m') \left(\frac{\partial \langle u_i \rangle'}{\partial x_j} \right) \left(\frac{\partial \langle u_j \rangle'}{\partial x_i} \right) (4.2)$$

From equation (4.2) we can see that the subgrid flux parameters K_m are used in the resolved part of the model. The first term in equation (4.2) is always negative and lowering c_f lowers K_m and thus lowers the resolved dissipation. This leads to more resolved motion. From this analysis, we can conclude that lowering c_f has positive effects on both resolved motion and subgrid motion: The subgrid fluxes are suppressed by a lower value of $K_{m,h}$ and the subgrid dissipation is enhanced. On the other hand, the resolved dissipation is decreased. The effects discussed here should make the resolved part of the model play a more dominating role than before. This can be observed in figure 4.18.

From figure 4.18 we can clearly see that although the subgrid part of the model remains the same, the resolved part of the model is much more important. This means that a bigger part of the SBL dynamics are directly calculated using the Navier-Stokes equation (2.3), instead of using the subgrid scale parameterization. This results is exactly what we are looking for, because, as mentioned in section 2.2, the LES provides only viable information if the resolved part is dominant.
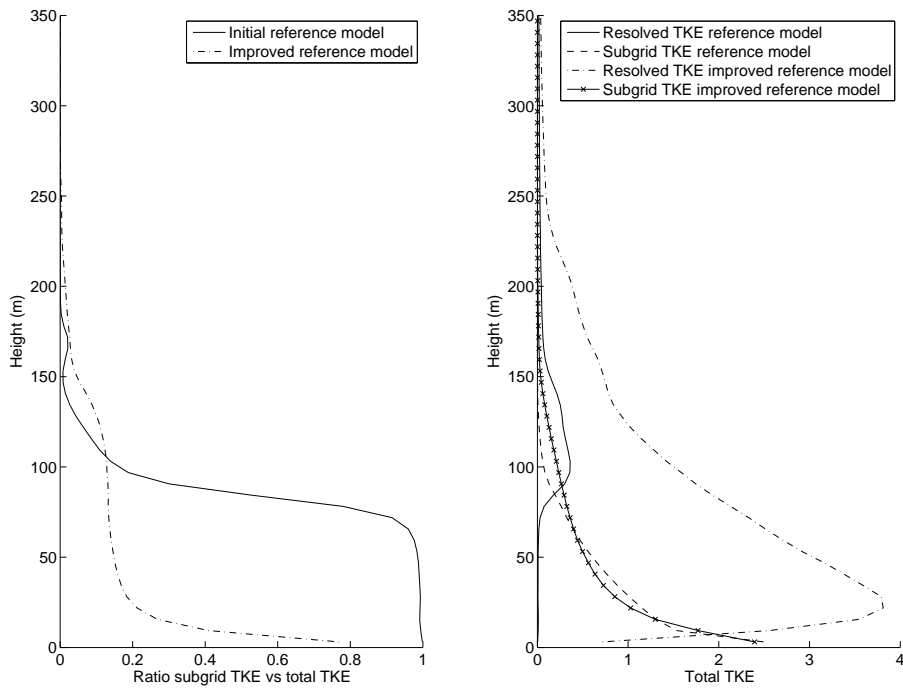
FIGURE 4.18: Ratio of the subgrid TKE versus the total TKE(left). Resolved and subgrid TKE (right)

Chapter 5

Sensitivity study to surface perturbations

We can now test our model by performing a sensitivity study to surface perturbations. In this section we will add a river or a ditch in the landscape with a different temperature and compare the results to the unperturbed model results, to investigate the effect of temperature perturbations on the dynamics of the SBL. As mentioned in chapter 3, adding a surface perturbation will increase the generation of turbulence. In order to make the two models comparable it is imperative that the mean surface temperature does not differ in the two cases. This means that

$$N_{total}T_{unperturbed} = N_{river}T_{river} + N_{land}T_{land} \tag{5.1}$$

where N_{total} is the total grid size, N_{river} the number of grid point used for the river and N_{land} the number of grid point which are not, and obeying the following rule: $N_{total} = N_{river} + N_{land}$. $T_{unperturbed}$ is the mean temperature of the homogeneous surface. T_{river} and T_{land} are respectively the temperature of the river and the temperature of the rest of the domain.

In order to avoid a *time* dependent temperature disturbance due to the river, a constant temperature difference between the river and the homogeneous surface will be maintained. This means that the river temperature will be maintained at a constant temperature difference with respect to the mean temperature.

5.1 Rotation results without surface perturbation

In our previous simulations we forced a wind of 8 ms^{-1} in the u direction. For computational reasons the rivers are also implemented in the u-direction. To maximize the effect of the temperature gradient and heat exchange created by the rivers, we will rotate the wind by 90°. By doing this the wind will not 'follow' the rivers but cross them. The wind will transport the heat from the river to the rest of the domain, and therefore increasing turbulence and horizontal mixing. Before simulating rivers in the improved LES model, we have rotated the field for the reasons mention before (i.e. maximizing the effect of the rivers). Rotating the wind field led to a surprising conclusions as can be seen from the next figure.
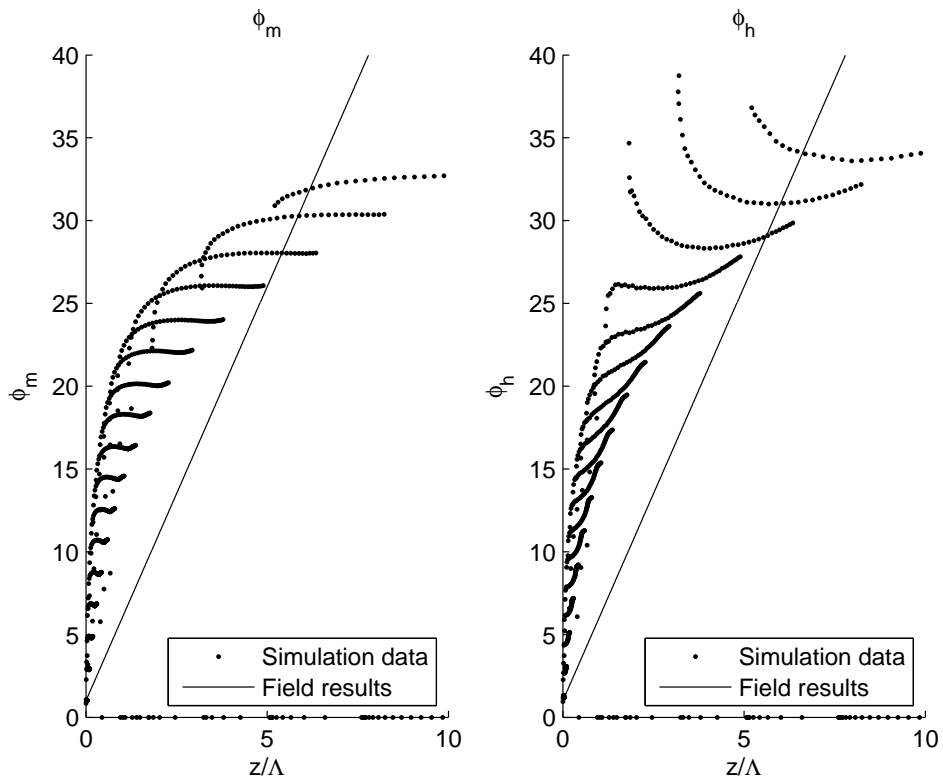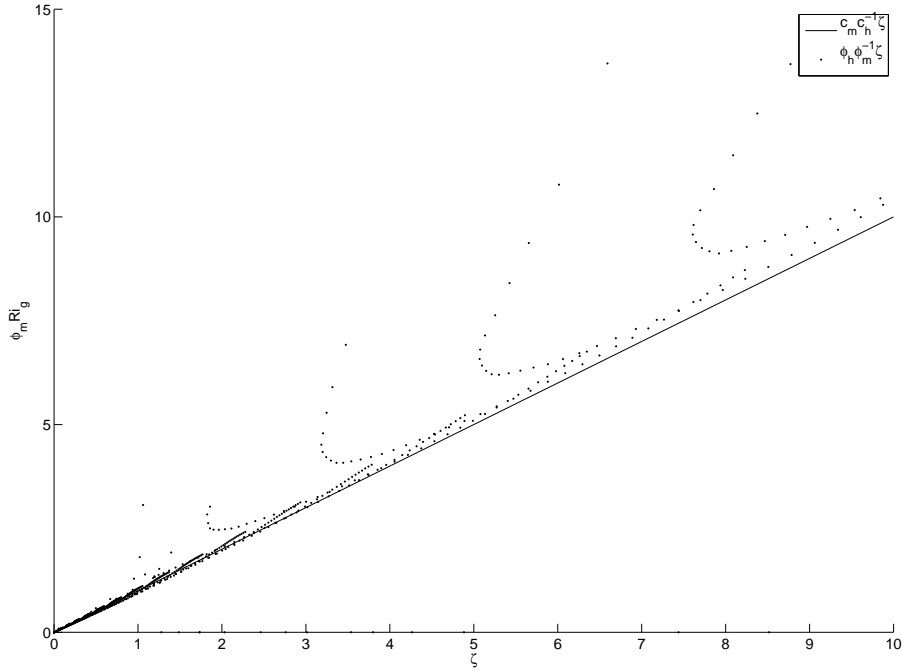
FIGURE 5.1: ϕ_m and ϕ_h relations with rotated wind field

FIGURE 5.2: $\phi_m Ri_g$ as a function of ζ for the rotated wind fields.

In figure 5.1 the relations ϕ_m and ϕ_h are plotted for the unperturbed state. As we can see, rotating the wind from the u-direction to the v-direction dramatically changes the dynamics of the atmosphere. Figure 5.3 ilustrates that the u and v component of the wind are definitely not interchangeable. Before starting to analyse let us first check if figure 5.1 is consistent with equation (2.29). From figure 5.2 we can see that the data is consistent with equation (2.29). Now let us take a look at the wind profiles. Naïvely it can be thought that the u and v component of the wind are interchangeable. In figure 5.3 both wind components are plotted in order to see if they are rotation invariant.

This can intuitively be explained by the Coriolis force present in the model. The Coriolis parameter is used in the steady-state momentum equation[5] and can be found as well in the Navier-Stokes equation (2.3):

$$\frac{\partial \overline{u}}{\partial t} = 0 = -\rho^{-1}\frac{\partial \overline{p}}{\partial x} + f\overline{v} - \frac{\partial \overline{(u'w')}}{\partial z} \tag{5.2}$$

$$\frac{\partial \overline{v}}{\partial t} = 0 = -\rho^{-1}\frac{\partial \overline{p}}{\partial y} - f\overline{u} - \frac{\partial \overline{(v'w')}}{\partial z} \tag{5.3}$$

Above the SBL, in absence of turbulence, equations (5.2) and (5.3) reduce to a balance between the Coriolis and the pressure-gradient. Substituting definitions (2.4) and (2.5) in equations (5.2) and (5.3) leads to

$$0 = f(\overline{v} - v_g) - \frac{\partial \overline{(u'w')}}{\partial z} \tag{5.4}$$
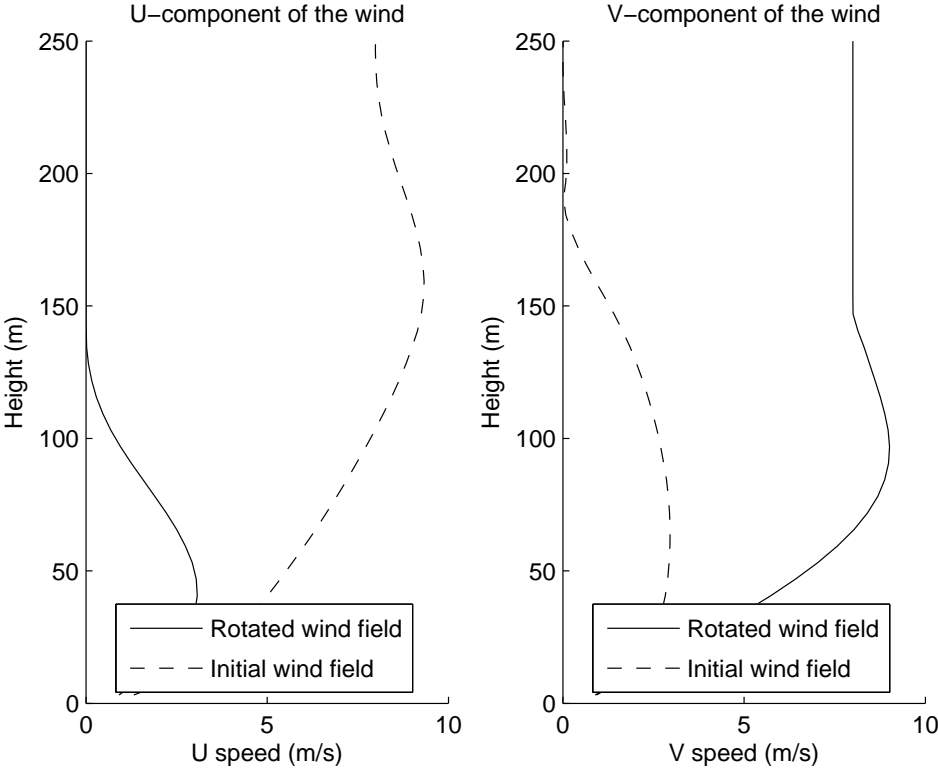
26

FIGURE 5.3: *u* and *v* component of the wind for both rotated and non-rotated wind field

$$0 = -f(\overline{v} - u_g) - \frac{\partial \overline{(v'w')}}{\partial z} \tag{5.5}$$

A minus sign in the previous equations explains why the u and v component of the wind are *not* interchangeable and thus why rotating the wind field changes the dynamics of the atmosphere. From now on the old wind field will be used, because a deep analysis of the effect of the rotation is required and this goes beyond the scope of this work.

5.2 Perturbation sensitivity

In the previous chapter we have substantially improved our reference model and we are now able to implement temperature differences in the surface in order to investigate the sensitivity of the model. For the temperature differences we have chosen the values $0.1°K$, $0.5°K$, $1°K$ and $1.5°K$. We have chosen these values to get a first impression and cover a broad range of perturbations. We have used a domain of 400m and a resolution of 6.25m in each direction, and the rivers (i.e. the temperature difference) has been set to one fourth of the domain. This has been done by cutting the domain in four pieces and attributing a temperature increase to one of them, and a temperature decrease to the rest of them, according to equation (5.1). According to Beare et al[2] a resolution of 6.25m will give reasonable accuracy and this resolution will also be used. Let us now analyse the results.

In figure 5.4 evolution in time of the temperature profile is plotted. First of all, we can see that by increasing the perturbation, we change the potential temperature profile dramatically. The potential temperature corresponding to a perturbation of $0.5°K$ and $1°K$ only varies a little with height, meaning that thermals at the surface will rise to almost the top of the domain, and leading to a significant vertical mixing. But as described in the case description gravity wave damping is applied above 300m and is now unphysically damping vertical motion. In order to bypass this problem, a simulation using a double vertical domain is a solution. When observing the evolution in time of the potential temperature profile of the simulation with a tenth of a degree of perturbation, we can see that a change in profile is started at the top of the domain. This is rather strange because a perturbation is applied at the *bottom* of the domain and not at the *top* of the domain. A numerical instability could be the result of this, and again, using a double vertical domain could solve this problem. What we have to keep in mind from this simulation, is that Beare used an a well mixed vertical layer at the bottom of the domain, this means that the temperature profile follows the adiabatic lapse rate $\Gamma_{adiabatic}$. This profile is favorable to generate turbulence. By adding temperature gradient at the surface we further enhance the turbulence, leading, in the case of a perturbation of $0.5°K$ $1°K$, to a well mixed layer *above* the SBL. This seems to be not physically acceptable and maybe this can be resolved by adding the river not at the beginning of simulation, but after the SBL has reach a (quasi-)steady state.
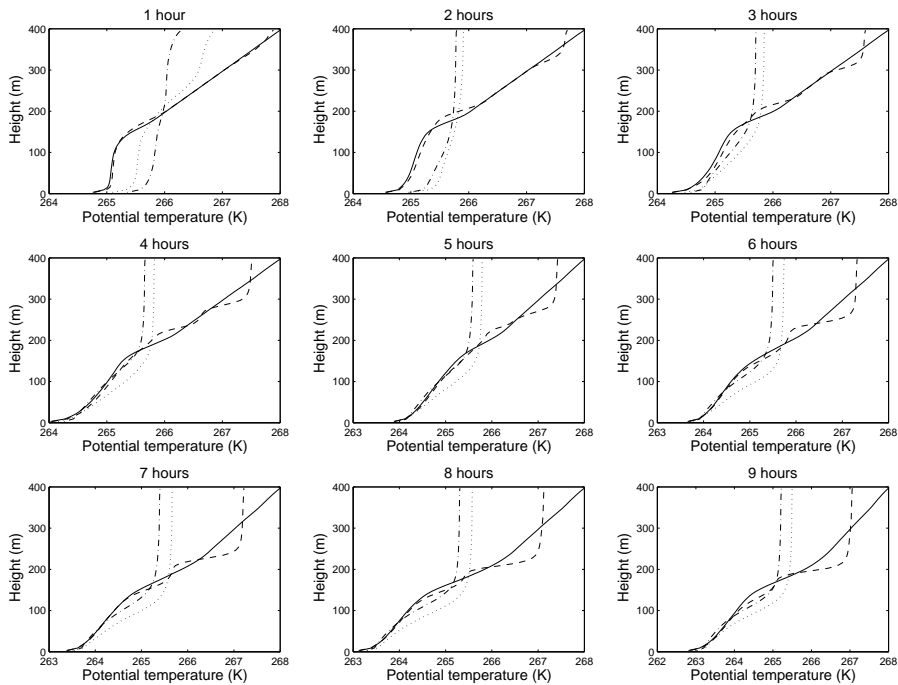
FIGURE 5.4: Time plotted wind profile for different surface perturbations. Solid line represents the unperturbed state, the dashed line a perturbation of $0.1°K$, the dotted line a perturbation of $0.5°K$ and the dash-dot line a perturbation of $1°K$

Chapter 6

Conclusion

The case studied here can be divided in two main parts, where the first one was mainly focusing on improving the LES model in order to be able to implement a temperature difference in the surface, which was the second part of this study. We have seen that the reference model could not simulate well the atmospheric evolution during stable conditions if we use a 6.25m grid resolution. This was caused by a very dominating subgrid solution and an almost absent resolved solution. A few changes has been made in the subgrid model in order to improve the final solution. The first one was forcing a Prandtl number of 1 as found in field experiments. This change has not an influence on momentum flux, which remains the same. But the buoyancy flux changes significantly. This is due to the fact that by forcing the Prandtl number to be one, the eddy diffusivity for the heat has changed as well, whereas the eddy viscosity for momentum was not affected by this change. Changing the Prandtl number has not significantly improved the model, it has only ensured that the flux-gradient relations ϕ_m and ϕ_h became equal ro each other as observed in reality. The next changes was changing the constant c_f, responsible for the value of the filter cutoff-frequency in the energy domain. This change is increasing subgrid dissipation, but it has not been observed that the subgrid solution was suppressed. Another effect on the subgrid model is the decrease of the subgrid fluxes by decreasing the eddy viscosity and the eddy diffusivity. By analysing the resolved part of the model and the subgrid TKE equation used to calculate the evolution of the atmosphere we demonstrated that changing c_f has an impact on the resolved solution by decreasing the resolves dissipation and thereby increasing the resolved motion. But the choice of the value of c_f is difficult to make, because the cutoff-wavelength of the filter is not the only parameter related to the subgrid energy. The form of the filter is also of a great importance. We can conclude that lowering c_f has indeed improved the LES model, but further study is necessary to find the optimal value of c_f to further improve the LES model. An interesting comparison can be made between the SBL as studied here and DNS results obtained by van de Wiel et al.[10]. By using a DNS simulation the same $\phi_{m,h}$ are obtained. This really astonishing because of the similarity on different scales (i.e. DNS $\sim$10cm).

In the sensitivity study to surface perturbations we have rotated the wind field in order to let the wind cross the rivers and not follow them. We discovered that rotating the wind has a significant effect on the dynamics, due to an asymmetry in the momentum equations. The Coriolis force is responsible for those changes. Further study is necessary

in order to investigate the impact of the geostrophic wind direction on the dynamic evolution of the atmosphere. A interesting observation was made when simulating rivers in our model. A temperature perturbation applied at the beginning of the simulation of 'only' $0.5K$ and $1K$ has a enormous effect on the potential temperature profile of the atmosphere. We can explain this by noting that we are using a vertically well mixed layer. When a parcel of air rises, it will follow the dry adiabatic lapse rate, and will rise until a negative buoyancy force slows it down. What is happening when we apply a surface perturbation, is that the air parcel above the river is hotter than its environment and will by this generate a lot more vertical speed. It will take longer to the buoyancy force to slow it down and thus will the air parcel reach a greater heigth, and can even escape the SBL. For this reason it is advisable to add the perturbation only when the SBL has reach a steady state situation, in order to observe the effect of the rivers only. But it is difficult to say when its most suited to add the temperature perturbation. As seen in figure 4.17, the SBL height reaches a steady state after 2 hours, but the momentum flux reaches a steady state after 4 hours (figure 4.16), and the buoyancy flux has not reach a steady state even after 9 hours. More research is needed on this.

Now will follow a short summary of the conclusions made during this study. Changing the turbulent subgrid Prandtl number from $\frac{1}{3}$ to has made 1 has been beneficial when analysing the ϕ_m and ϕ_h relations. Further improvement has been made by changing the filter constant c_f from 2.5 to 2. This change has made simulation results agree with field measurements, but further study is needed to find the optimal value of c_f. Sensitivity study has revealed that the direction of the geostrophic wind has a great impact on the SBL dynamics, due to the Corioli force. Further research is needed to understand the consequences this can have on further LES developments. We can also conclude that a surface temperature perturbation increases the overall turbulence in the atmosphere, but more research is needed to investigate, for example, the effect of the wind speed and direction on the perturbation, the impact of the amplitude of the perturbation and the effect of the area of the perturbation on the overall dynamics.

Bibliography

1. P. Baas and S.R. de Roode. The scaling behaviour of a turbulent kinetic energy closure model for stably stratified conditoins. *Boundary-Layer Meteorol.*, 2007.

2. R.J. Beare. An intercomparison of large-eddy simulations of the stable boundary layer. *Boundary-Layer Meteorol.*, 118:247–272, 2006.

3. P.G. Duynkerke and S.R. de Roode. Surface energy balance and turbulence characteristics observed at the sheba ice camp during fire III. *J. Geophys. Res.*, 106:15313–15322, 2001.

4. A. Dyer. A review of flux-profiel relationships. *Boundary-Layer Meteorol.*, 7:363–372, 1974.

5. J. R. Garatt. *The Atmospheric Boundary Layer.* Cambridge University Press, 1992.

6. P. Mason. Large-eddy simulation of the convective atmospheric boundary layer. *Journal of Atmospheric Sciences*, 46:1492–1516, 1989.

7. F. T. M. Nieuwstadt. The turbulent structure of the stable, nocturnal boundary layer. *J. Atmos. Sci.*, 41:2202–2216, 1984.

8. S.R de. Roode. Derivation of the prognostic equation for $\overline{u_i'^2}$. Unpublished.

9. S. R. de. Roode. The steady-state subgrid TKE solution for stable stratification. Unpublished.

10. B. van de Wiel, A. Moene, W. D. Ronde, and H. Jonker. Local similarity in the stable boundary layer and mixing-length approaches: Consistency of concepts. Boundary-Layer Meteorology, 2008.

11. M. v. Zanten. *Entrainment processes in stratocumulus.* PhD thesis, Utrecht University, 2000.

12. S. S. Zilitinkevich and I. Essau. Similarity theory and calculation of the turbulent fluxes at the surface for the stably stratified atmospheric layer. *Boundary-Layer Meteorol.*, 125:193–205, 2007.